Assessment of TERRA-ASTER and RADARSAT imagery for discrimination of dunes in the Valdes peninsula: an object oriented approach

P. D. Blanco[1] , G. I. Metternicht[1], H. F. del Valle[2] y W. Sione[3,4]

blanco@cenpat.edu.ar

(1) Centro Nacional Patagónico-CONICET, Boulevard Brown 2825, U9120ACF, Pto Madryn, Argentina
(2) School of Natural and Built Environments, University of South Australia, 5095, Mawson Lakes, SA
(3) CEREGeo-FCyT/UADER, Ruta 11 Km 10, 3100, Oro Verde, Entre Ríos, Argentina
(4) PRODITEL-Universidad Nacional de Luján, Cruce rutas ex. 5 y 7, 6700, Luján, Bs As, Argentina

RESUMEN

Areas como Península Valdés (Patagonia Argentina), Patrimonio de la Humanidad desde 1999, están sujetas a degradación del suelo por acción eólica y sobrepastoreo. La cartografía de indicadores de degradación del paisaje, como dunas activas activas y estabilizadas, es crucial para mejorar la predicción, monitoreo y manejo de suelos afectados. Este trabajo compara clasificaciones basadas en el objeto y en el píxel para la discriminación de dunas activas y estabilizadas, y evalúa las diferencias en la fiabilidad de la clasificación al usar la sinergía de ASTER y Radarsat.

PALABRAS CLAVE: segmentación multi-resolución, clasificación orientada al objeto, Terra-ASTER, Radarsat-ASAR, Patagonia.

ABSTRACT

Areas like the Peninsula Valdes (Patagonia Argentina), declared a World Heritage site in 1999, are subject to soil degradation by wind and overgrazing. Mapping landscape degradation indicators such as stabilized and active dunes is critical to improve prediction, monitoring and planning of areas threatened by sand encroachment. To this end, this paper investigates the contribution of optical sensors like the Terra-ASTER and the microwave Radarsat ASAR to the discrimination of these land degradation features.

KEY WORDS: multi-resolution segmentation, object-oriented classification, Terra-ASTER, Radarsat-ASAR, Patagonia.

INTRODUCTION

Arid and semiarid drylands compose nearly a one-third of the land surface of the world (OIES, 1991). It is estimated that 50% to more than 70% of these areas are degraded as a result of overgrazing, aggravated by the characteristics of dryland climates (Warren & Agnew, 1988). Areas like Península Valdés (southern Argentina), declared a UNESCO World Heritage site in 1999, are subject to soil degradation by wind and overgrazing. Mapping and monitoring the presence of landscape degradation indicators such as stabilized and active dunes is crucial to improve prediction, and for monitoring and planning of areas threatened by sand encroachment.

Satellite remote sensing is an effective tool for mapping landforms in a rapid and accurate manner. Visible-infrared (VIR) data can be used to discriminate active and stabilized dunes based on the distinctive reflectance values of light-colored sands (proper of active dune areas) and dark-colored vegetation, which produce significant tonal differences in the re-

mote sensing imagery (e.g., Paisley et al., 1991). Synthetic Aperture Radar (SAR), in contrast to VIR, is an active form of remote sensing. Radar images have the potential to provide information on the geometry of sand dunes and other aeolian features because of the radar sensitivity to changes in the structure of surficial features (Blumberg, 1998). Thus, by merging optical and radar data, an additional portion of the spectrum is available, which may improve classification.

Classification based on individual pixels is generally unsatisfactory for arid landforms that often consist of highly variable mixtures of scattering objects, and are largely distinguished by their spatial, besides their spectral, characteristics. Hence, much information is contained in the relationship between adjacent pixels, including shape, texture, relational and contextual information, which allows for identification of individual objects as opposed to single pixels (Thomas et al., 2003). Pixels are aggregated into image objects by segmentation, which is defined as the division of remotely sensed images into discrete regions or objects that are homogenous with regard to spatial or spectral characteristics (Ryherd & Woodcock, 1996). Object-based segmentation and image classification techniques are receiving increasing attention for widespread application to the classification of visible, infrared and microwave data (e.g., Laliberte et al., 2007). To this end, in this research we aimed to:

(1) Map active and inactive dunes by using visible/infrared sensors like the Advanced Spaceborne Thermal Emission and Reflection Radiometer (ASTER) on-board the Terra platform;

(2) Assess accuracy improvements in the detection of dunes by incorporating microwave Radarsat SAR data; and

(3) Compare the results of a per pixel classification against an object-oriented approach for the mapping of active and stabilized dunes.

METHODOLOGY

Study area

Our study was conducted in Península Valdés (lat 42º32'S, 63º54'W), Patagonia Argentina (Fig. 1). The climate is semiarid, with an annual mean temperature of 13ºC, and average annual rainfall of 231 m.
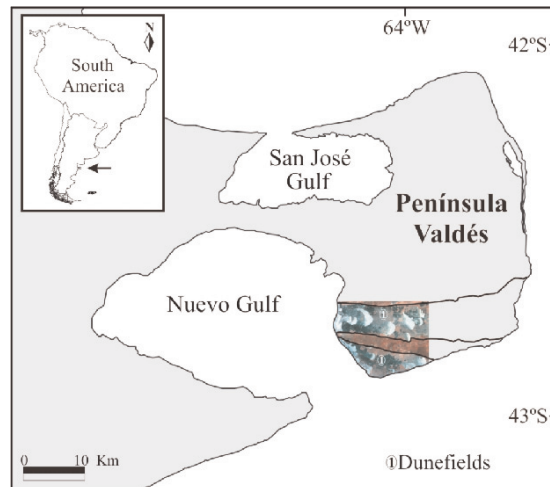

Figure 1. Study area location. ASTER composite, bands 3, 2, 1.

Mean annual wind speed is 25 km•h-1, with prevailing winds from the west and north-west.

Two dunefields are distinguishable in Península Valdés: the largest one is located in the central area forming a belt that stretches from the west to the east coast, and the smaller one is a fringe-like dunefield in the southwest corner of the peninsula. General features in the topography of the dunefield are relic aeolian landforms, megapatches of active sand dunes and erosional features like regs and blowouts. Megapatches of active sand dunes include barchan, dome and transverse dunes. Relict aeolian landforms include sand sheets and lineal dunes stabilized by psammophile species.

The vegetation is transitional between Monte and Patagonian Phytogeographic Provinces (León et al., 1998). Vegetation covers 50 to 80% of the dunefields, with the most widespread communities being grasslands of Sporobolus rigens, Panicum urvilleanum and Stipa tenuis; and scrublands dominated by Hyalis argentea. A shrub steppe of Chuquiraga avellanedae extends between both dunefields, but this area were not including in this study.

Using pre-existing physiographic and vegetation maps, and information on current field situation, six dominant vegetation-landforms patterns were identified in the study area. These are: Active dune, Reg, Grassland, Grass Stabilized Lineal Dune, Scrubland, and Scrub Stabilized Lineal Dune.

Research approach

The research approach encompasses the following steps:
1) Identification of landscape features related to the

presence of active and stabilized dunes. Two vegetation types are considered as dune stabilizers: scrub and grass;

2) Calibration and georeferencing of the Terra-ASTER imagery, including the computation of spectral indices and principal component analysis for the removal of redundant spectral information;

3) Despeckle and georeferencing of a precision mode Radarsat imagery;

4) Creation of a geo-spatial soil database to store field observations and spectral characteristics of wind-erosion related features in the optical and microwave regions of the spectrum;

5) Extraction of Radarsat derived textural measures;

6) Classification of the selected imagery using a per-pixel maximum likelihood algorithm in ERDAS Imagine software;

7) Segmentation and object-oriented classification using eCognition software;

8) Accuracy evaluation of the resulting classifications using error matrices and Kappa sta-tistics.

Image pre-processing

The ASTER level 1B scene was acquired on 27th November 2004, georeferenced to a UTM projection, WGS-84 ellipsoid, and converted to radiance values. ASTER acquires data in 3 separate subsystems: VNIR (bands 1, 2, 3, SR=15 m), SWIR (bands 4-9, SR=30 m), and TIR (bands 10-14, SR=90 m). Given the high correlation between bands (above 0.9) a PCA was applied to remove redundant information. The first two components explained 98% of the image variability, and thus they were selected for further analysis. The ASTER VNIR and SWIR band 4 showed the highest contribution to these first two components, and thus were selected as the raw bands to be included in the classification process. The Soil Adjusted Vegetation Index (SAVI), designed to minimize the effect of the soil background (Huete 1988), was computed as a means to gather information on vegetation cover. SAVI was applied to the ASTER data set using the following equation:

Figure 2. Radarsat-1 ASAR image showing part of the study area. The brightness tones represent backscatter magnitud values.

$$SAVI = \left[\frac{(A_3 - A_2)}{(A_3 + A_2 + L)} \right] * (1 + L)$$

Where A_2 and A_3 are the radiance values corresponding to the ASTER bands 2 (red) and 3 (NIR), respectively; and L is and adjustment factor. Similarly to the Normalized Difference Vegetation Index (NDVI), the near infrared and red bands are used in the calculation of SAVI, but with the addition of an adjustment factor (L), which varies between zero and one. We used an adjustment factor of 0.5, which has been shown to reduce soil influences considerably (Huete 1988) and is the most widely used adjustment factor for intermediate vegetation cover.

The Radarsat-1 ASAR image, C-band, HH polarization, was acquired on the 1st January 2005, in fine mode 4, with a spatial resolution of 8 m (Fig. 2). The raw data was converted to magnitude image products, filtered to decrease speckle noise characteristic of SAR images using a Frost filter and georeferenced to a UTM projection. Textural measures derived from the Grey Level Co-occurrence Matrix (GLCM) were used to ascertain their value for mapping active and stabilized dunes (Haralick, 1973). Measures of mean, variance, contrast, and dissimilarity were implemented in the Radarsat imagery.

Subsequently, image to image registration was conducted between the ASTER and Radarsat images in order to keep registration errors to less than half a

pixel. To this end, a nearest neighbour resampling algorithm and output pixel size of 8 m were used. Bands 1 to 4 from the ASTER and the selected Radarsat-derived texture measures were stacked into one single image for a multi-sensor analysis (ERDAS, 2003).

Pixel based classification

For the pixel based classification, a standard maximum likelihood classifier as featured in the software Erdas Imagine was used. The functionality of the pixel-based classification is not explained here in detail, but it can be found in standard image processing textbooks like Chuvieco (2002). The number of training pixels was 486 for Active Dunes, 279 for Reg, 243 for Grassland, 252 for Scrubland, and 558 and 531 for Lineal Dunes Stabilized by Grass and Scrub, respectively.

Object-oriented approach

The procedure outlined in Figure 3 can be divided into two major parts. First, the multi-segmentation of the input data is performed. This procedure generates highly homogeneous segments in a selectable resolution and of a comparable size. Classification is then performed using those objects rather than single pixels. The classification of the image objects can be performed by using nearest neighbour classifiers based on user selected samples or by using fuzzy membership functions (Zadeh, 1965), with user-defined rules. A fuzzy membership ranges from 0 to 1 for each object's feature values with regard to the object's assigned class. Spectral, shape, and statistical characteristics as well as relationships between linked levels of the image objects can be used in the rule base to combine objects into meaningful classes (Benz et al. 2004).

Two image segmentation trials were implemented using different input data sets (Table 1).The first trial used the four raw ASTER bands (1 to 4); whereas the second integrated spectral and texture information (i.e. mean, variance, contrast and dissimilarity co-occurrence texture images) derived from Radarsat data. The object oriented approach considers three parameters for image segmentation, namely scale, colour/shape ratio, and smoothness/compactness ratio. The weights for colour and shape were established after several iterations to a ratio of 0.8:0.2 for the relative importance of colour versus shape, and 0.1:0.9 for compactness versus smoothness.

The image classification followed a three-levels approach (Figure 4), whereby the third level, segmented on the coarse scale, used a SAVI threshold for the separation of broader land covers (e.g. objects with a SAVI of less than 0.74 were considered to be dune fields; whereas objects with digital numbers above 0.74 were classed as Shrub Steppe). A separation amongst the classes Grassland, Scrubland and Areas Not-Vegetated was achieved using a nearest neighbour classification, based on the training chosen in the SAVI feature space. The second level aimed at identifying active dunes by defining fuzzy membership functions for mean brightness values, related to the input data of each trial (Table 1). Two subclasses of the Active Dune, namely AD-1 and AD-border, were defined. Then, an object fusion was applied to group the objects of these classes under the general class, active dunes. The Reg class was considered complementary to actives dunes.

Lastly, the first level was designed to extract areas of stabilized dunes. To this end, we discriminated between dunes stabilized by grass and dunes fixed by scrub, defining the classes GSD-1 and SSD-1 based on membership functions for mean brightness values. Because these classes had similar brightness values and could be confused with other classes, we established a restriction on the shape of the segments: the length/width ratio should be bigger than four. In order to integrate wrongly excluded objects two new subclasses were defined, GSD-border and SSD-border, which had the brightness feature space broader but with the constraint that the relative border length to GSD-1 and SSD-1, respectively, was greater than one. The Grassland and Scrubland classes were defined as complementary of those classes, respectively.

Accuracy assessment

The accuracy assessment was done by means of an error matrix based on stratified and randomly selected sites across the study area. The ground truthing was carried out by field survey in the summer of 2005 visiting as many sites as possible, and confirming the vegetation-landform type in situ with a
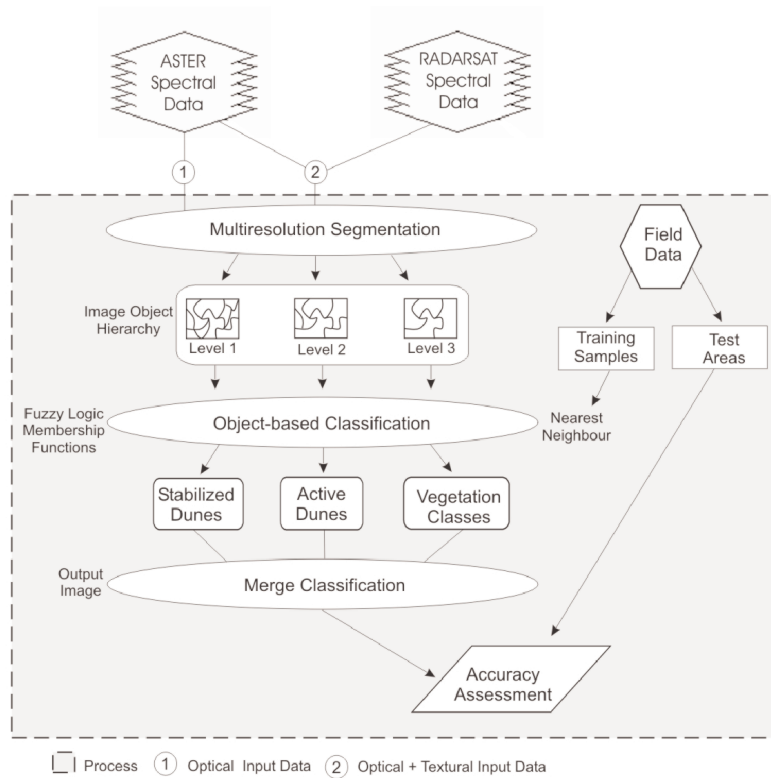
Inputs	Scale		
	Level 1	Level 2	Level 3
B1-4 ASTER	3	7	9
ASTER & Textural Data	8	15	25

Table 1. Input datasets used in the trials.

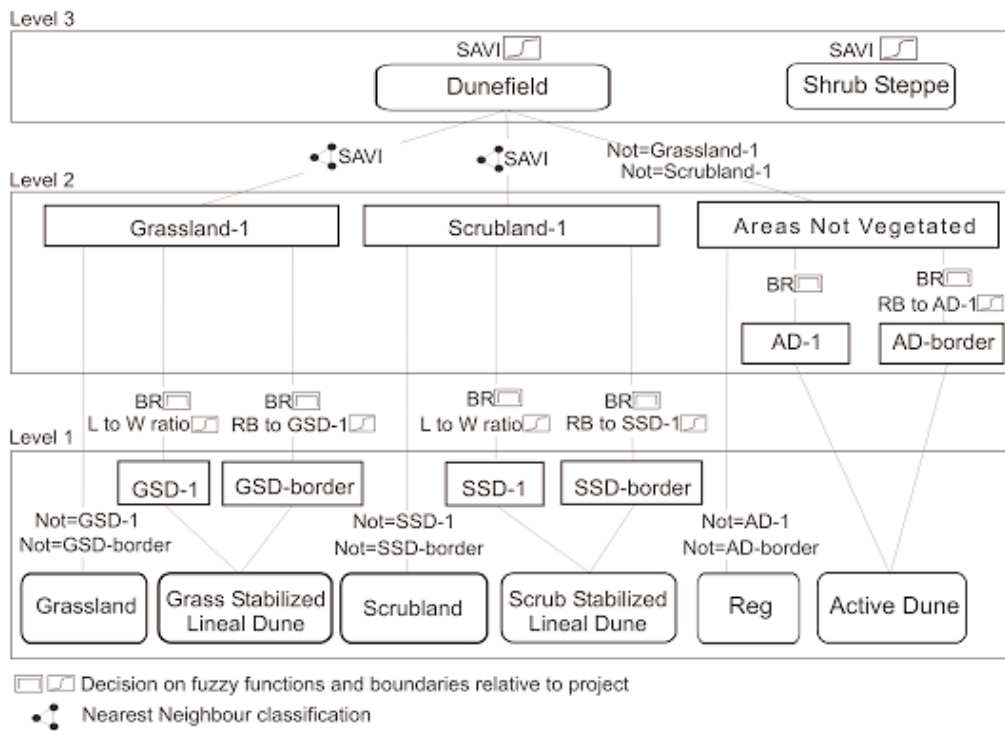**Figure 3.** Conceptual model of the object oriented approach adopted in this study.

Figure 4. Fuzzy membership functions for all the classes. BR denotes brightness, L to W means the ratio Length/Width and RB is the relation of border to a certain class.

Global Positioning System (GPS) unit. At each validation site, an area of 45 by 45 m was examined, to account for location errors caused by positional inaccuracies of the GPS and/or the geometric correction of the satellite imagery. The number of validation pixels was 729 for Active Dune, 414 for Reg, 369 for Grassland, 360 for Scrubland, and 837 and 792 for Lineal Dunes Stabilized by Grass and Scrub, respectively.

Error matrices were used as the basis for calculating the overall accuracy, individual class user's and producer's accuracy, KHAT statistic and its variance (an estimate of the kappa coefficient) (Congalton, 1991). The efficiency of the synergistic approach was evaluated with a kappa analysis. KHAT statistic and its variance were used to construct a hypothesis test for statistically significant difference between error matrices (Cohen, 1960), being the null hypothesis that there is no disagreement between the KHAT values.

DISCUSSION OF RESULTS

Per pixel classification of the ASTER data

The first step was to analyse the separability of the classes of interest using a maximum likelihood classifier as featured in the ERDAS Imagine software. The scatter plot (Fig. 5) shows significant overlaps between the classes Active Dune and Reg, as well as Grassland and GSD, and between Scrubland and GSD.

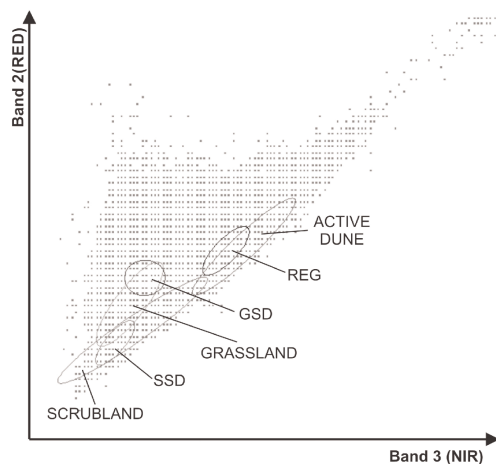These results are consistent with the classification outputs shown in Fig. 6. The ASTER-derived spectral signatures for lineal dunes and the different semi-arid vegetation types do not differ greatly, returning spectrally similar responses. They have similar average digital numbers (DNs) and all possess high standard deviations. This creates areas of overlap in their spectral signatures, which causes confusion, and limits their spectral separability. The class Active Dunes shows a higher average DN, which improves its spectral discrimination from the inactive dunes, though exhibiting a high standard deviation that creates areas of overlap with the Reg class. The final classification result has an overall accuracy of 52.7%, and a KHAT equal to 43.4%. According to Congalton (1991) kappa values can be subdivided into 3 groups, where a value greater than 0.80 (80%) represents strong agreement, a value between 0.40 and 0.80 (40 to 80%) represents moderate agreement, and a value below 0.40 (40%) represents poor agreement. Adopting this standard, the accuracy achieved by the per pixel classification represents a moderate agreement. Both the user's and producer's accuracies for the classes were low too (results are not shown), as they had nearly the same number of pixels confused with the other classes as they have correctly classified.

Object-oriented classifications

The high standard deviation associated with the ASTER-derived thematic classes suggests that the inclusion of textural measures may increase the discriminatory ability of the optical sensor. Figures 7
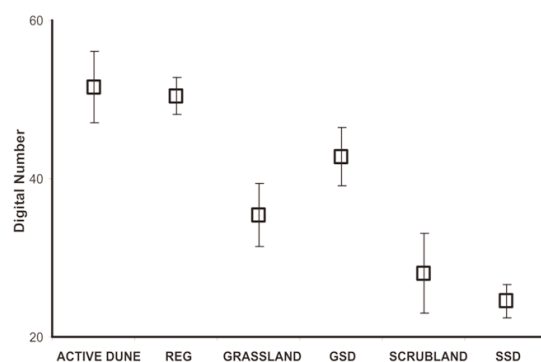

Figure 5. Scatter plot of the maximum likelihood classification.

Figure 6. Spectral signatures (mean ± 1 standard deviation) of the different thematic classes in the green band 1 of the ASTER scene.
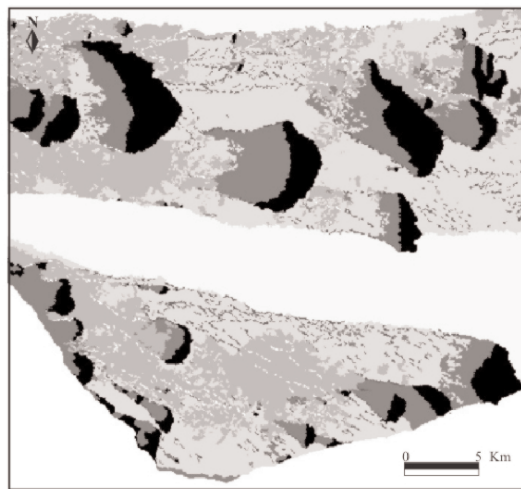
Figure 7. Cartography of soil degradation indicators using and object-oriented classifier on the 1-4 bandsASTER dataset.

Legend: Active Dune, Reg, Grassland, GSD, Scrubland, SSD, Shrub Steppe

Figure 8. Object-oriented cartography of soil degradation indicators using the fusion of ASTER and Radarsat-derived textural data.

Legend: Active Dune, Reg, Grassland, GSD, Scrubland, SSD, Shrub Steppe

and 8 show the results of using an object-oriented classification on the visible/infrared data from the Terra-ASTER, and integrated spectral and textural image information (as derived from the Radarsat ASAR data), respectively.

Accuracy assessments for the ASTER data set classified alone, and the integrated ASTER and Radarsat-derived texture data are presented in tables 2 and 3, respectively. The KAPPA analysis result for the pairwise comparison between the ASTER and integrated ASTER and textural information shows a result of 5.96, which is superior to 1.96 (the critical value at the 95% confidence level), revealing that the two error matrices are significantly different.

Kappa statistics above 80%, with 3 classes showing above 90% accuracy of discrimination, are achieved when mapping the six classes of interest using the synergy of spectral and textural data derived from ASTER and Radarsat imagery (Table 3). A comparison of the classification accuracies obtained with the different layer combinations revealed that the integrated ASTER and Radarsat-derived textural data produced better overall accuracy and a higher KHAT statistic value than the classifications resulting from the ASTER data alone, implying that the synergistic approach enabled better discrimination of the land degradation features in the study area.

These results suggest an improvement in the classification of active dunes and stabilized dunes (vegetated by either scrub or grass) is achieved by using an object-oriented classification that integrates tex-
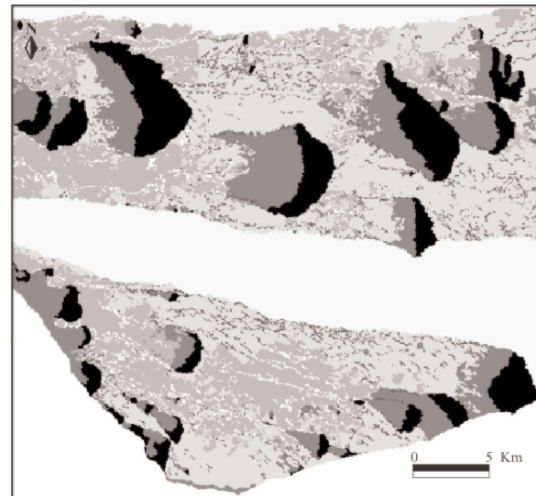
tural information derived from microwave imagery and optical/IR data from Terra-ASTER. It appears that changes in surface roughness caused by different vegetation types stabilizing the dunes is a major influence in radar backscattering. For instance, Radarsat imagery enables a clear separation of long and narrow dunes stabilized by scrub against those stabilized by grass, the former showing a higher classification accuracy. On the other hand, ASTER optical and infrared wavebands show superior performance in the cartography of grass-stabilized dunes. It also appears that the synergistic use of microwave, optical and infrared data increases substantially the accuracy in the discrimination and mapping of soil degradation features related to wind erosion.

The object-based classification technique used in this study proved a valuable tool and was suitable for optical and radar data classification. Objects of similar spectral reflectance and radar backscatter, as stabilized lineal dunes, could be discriminating by describing differences between neighbouring objects as well as objects on a different hierarchical level. In addition, the object-oriented classifier allowed interpreting each decision rule and make efficient use of only important object's features for the classification. Future related research will include application of the technique over larger areas; comparison with other classifiers, including neural networks and decision trees approaches; and analysis of the influence of image date on the approach proposed.

For the stabilized and active dunes discrimination,

Class	AD	REG	G	GSD	S	SSD	UA
AD	666	36	0	0	0	0	95
REG	63	360	0	27	0	18	77
G	0	0	324	153	0	0	68
GSD	0	0	45	657	0	0	94
S	0	18	0	0	333	216	59
SSD	0	0	0	0	27	558	95
PA	91	87	88	79	92	70	OA 82.8%
KHAT	89	85	86	73	91	64	KHAT 79.1%

AD: Active dune; G: Grassland; GSD: Grass stabilized dune; S: Scrubland;
SSD: Scrub stabilized dune. UA: User's accuracy; PA: Producer's accuracy

Table 2. Accuracy assessment of the ASTER object-oriented classification.

Class	AD	REG	G	GSD	S	SSD	UA
AD	684	36	0	0	0	0	95
REG	45	378	0	18	0	18	82
G	0	0	306	90	0	0	77
GSD	0	0	63	729	0	0	92
S	0	0	0	0	342	72	83
SSD	0	0	0	0	18	702	98
PA	94	91	83	87	95	87	OA 89.7%
KHAT	92	90	81	83	94	86	KHAT 87.4%

AD: Active dune; G: Grassland; GSD: Grass stabilized dune; S: Scrubland;
SSD: Scrub stabilized dune. UA: User's accuracy; PA: Producer's accuracy

Table 3. Accuracy assessment of the combined ASTER-Radarsat derived textural data classified using an object-oriented approach.

the results showed the horizontal-horizontal (HH) polarization radar data in C-band are appropriate for dune identification with an acceptable rate of correct classification (around 90%). Nevertheless, the use of multi-frequency polarimetric data can be expected to produce more information about surface roughness than can be obtained from a single waveband. The performance of texture measures derived from cross-polarized C- and L-band data needs further investigation.

ACKNOWLEDGMENTS

REFERENCIAS

HOLBEN, B.N., 1986. Characteristics of maximum values composite image from temporal AVHRR data. *International Journal of Remote Sensing,* 1986, Vol.7, 1417-1434.

HOLBEN, B.N., 1986. Characteristics of maximum values composite image from temporal AVHRR data. *International Journal of Remote Sensing,* 1986, Vol.7, 1417-1434.

HOLBEN, B.N., 1986. Characteristics of maximum values composite image from temporal AVHRR data. International Journal of Remote Sensing, 1986, Vol.7, 1417-1434.

HOLBEN, B.N., 1986. Characteristics of maximum values composite image from temporal AVHRR data. *International Journal of Remote Sensing,* 1986, Vol.7, 1417-1434.

BENZ, U.C., HOFFMANN, P., WILLHAUCK, G., LINGENFELDER, I., HEYNEN, M. 2004. Multi-resolution, object-oriented fuzzy analysis of remote sensing data for GIS-ready information, *ISPRS Journal of Photogrammetry and Remote Sensing*, 58:239–258.

BLUMBERG, D.G., 1998. Remote sensing of desert dune forms by polarimetric synthetic aperture radar (SAR). *Remote Sensing of Environment,* 65:204– 216.

CHUVIECO, E., 2002. *Teledetección Ambiental: La observación de la Tierra desde el Espacio.* Barcelona:Ariel Ciencia.

COHEN, J. 1960. A coefficient of agreement for nominal scales. *Educational and Psychological Measurement,* 1:37-40.

CONGALTON, R. 1991. A Review of Assessing the Accuracy of Classifications of Remotely Sensed Data. *Remote Sensing of Environment* 37:35-46.

ERDAS INC. 2003. ERDAS, Version 8.7. Available at: http://www.erdas.com/.

HARALICK, R. M., SHANMUGAM, K., DINSTEIN, I., 1973. Texture feature for image classification. *IEEE Transactions on Systems, Man, and Cybernetics,* 3:610- 621.

HUETE, A.R., 1988. A soil-adjusted vegetation index (SAVI), *Remote Sensing of Environment*, 25:295-309.

LALIBERTE A. S., FREDRICKSON, E. L., RANGO, A., 2007. Combining decision trees with hierarchical object-oriented image analysis for mapping arid rangelands. *Photogrammetric engineering & Remote sensing.* 2:197-207.

LEON, R.J.C., BRAN, D., COLLANTES, M., PARUELO, J.M., SORIANO, A., 1998. Grandes unidades de vegetación de Patagonia extra andina. *Ecología Austral.* 8:75-308.

OIES, 1991. Arid ecosystem interactions. Boulder, CO: Office of Interdisciplinary Earth Studios.

PAISLEY, E.C.I., LANCASTER, N., GADDIS, L.R., GREELYE, R., 1991. Discrimination of active and inactive sand from remote sensing: Kelso Dunes, Mojave Desert, California. *Remote Sensing of Environment,* 37:153–166.

RYHERD, S., WOODCOCK, C. E., 1996. Combining spectral and texture data in the segmentation of remotely sensed images. *Photogrammetric Engineering and Remote Sensing,* 62:181–194.

THOMAS, N., HENDRIX, C., CONGALTON, R. G., 2003. A comparison of urban mapping methods using high-resolution digital imagery. *Photogrammetric Engineering and Remote Sensing*, 69: 963– 972.

WARREN, A., AGNEW, C., 1988. An assessment of desertification and land degradation in arid and semi-arid areas. *Drylands Programme Research.* Paper No.2. London: IIED.

ZADEH, L.,1965. Fuzzy sets. Information Control, 8:338–353.